Shear layers in the turbulent pipe flow of drag reducing polymer solutions

I. Zadrazil, A. Bismarck, G.F. Hewitt, C.N. Markides*

Department of Chemical Engineering, Imperial College London
South Kensington Campus, SW7 2AZ, London, UK

Abstract

A range of high molecular weight polymers (polyethylene oxide) was dissolved at very low concentrations – in the order of few wppm – in a solvent (water). The Newtonian character of the polymer solutions was confirmed by rheological measurements. The polymer solutions were then pumped through a long horizontal pipe section in fully developed turbulent conditions. The flow experienced a reduction in frictional drag when compared to the drag experienced by the equivalent flow of the pure solvent. Specifically, drag reduction was measured at Reynolds numbers ranging from 3.5×10^4 to 2.1×10^5 in a pressure driven flow facility with a circular tube section of internal diameter 25.3 mm. The turbulent flow was visualized by Particle Image Velocimetry and the resulting data is used to investigate the effect of the drag reducing additives on the turbulent pipe flow. Close attention was paid to the mean and instantaneous velocity fields, as well as the two-dimensional vorticity and streamwise shear strain rate. The results indicate that drag reduction is accompanied by the appearance of "shear layers" (i.e. thin filament-like

*Corresponding author. *Telephone*: +44 (0)20 759 41601
Email address: c.markides@imperial.ac.uk (C.N. Markides)

regions of high spatial velocity gradients) that act as interfaces separating low-momentum flow regions near the pipe wall and high-momentum flow regions closer to the centerline. The shear layers are not stationary. They are continuously formed close to the wall at a random frequency and move towards the pipe centerline until they eventually disappear, thus occupying or existing within a "shear layer region". It is found that the mean thickness of the shear layer region is correlated with the measured level of drag reduction. The shear layer region thickness is increased by the presence of polymer additives when compared to the pure solvent, in a similar way to the thickening of the buffer layer. The results provide valuable insights into the characteristics of the turbulent pipe flow of a solvent containing drag reducing polymers that can be used to further our understanding of the role of polymers on the mechanism of drag reduction and to develop advanced drag reduction models.

Keywords: Drag reduction, hydrodynamics, pipe flow, polymers, turbulence, visualization

---

1. Introduction

It is well known that the frictional resistance caused by turbulent flow of a Newtonian fluid (solvent) in a pipe can be considerably reduced by the addition of a polymer to the solvent (Toms, 1948). An important consequence of this phenomenon, known as drag reduction, is that a fluid (liquid) solution containing the polymer additive will exhibit a lower pressure drop in a pipe flow compared to the pure solvent at the same flow-rate. The phenomenon of drag reduction occurs exclusively in turbulent flow and is of great industrial importance. Specifically, it is relevant in a broad array of applications that involve liquid transport through pipelines (Burger et al., 1980), ranging from fire fighting to field irrigation (Singh et al., 1995) and flows in urban sewage networks (Sellin et al., 1980), hydraulic fracturing (Lucas et al., 2009; Morgan et al., 1990), oil pipeline systems and secondary oil well operations.

Polymers have been identified as the most efficient drag reducers with respect to other drag reduction additives such as surfactants or bubbles (Bismarck et al., 2005). The amount of polymer additive required to alter the turbulent flow structure is in the order of few parts per million by weight (wppm). Drag reduction was for example observed for polymer concentrations as low as 0.02 wppm (20 wppb) by Oliver et al. (1983).

Virk et al. (1967) was the first to propose an important universal asymptote of maximum drag reduction, sometimes called Virk's asymptote, which is independent of experimental set-up or polymer additive. In a follow-up paper Virk (1975) established common characteristics of velocity profiles associated with the turbulent flow of polymeric solutions. An increasing presence of polymer additives was found to be associated with a thickening of the

buffer layer and a shift of the log-law region away from the Newtonian law of the wall, or viscous sublayer. At maximum drag reduction the buffer layer was found to extend to the centerline and the log-law region disappeared.

Drag reduction has been studied extensively since its discovery (Brostow, 2008; Lumley et al., 1998; Virk, 1975; White et al., 2008), but direct phenomenological insight into the effect of polymer additives on the turbulent flow intensity and structure was lacking until recently when non-intrusive flow visualization techniques were used (den Toonder et al., 1997; Ptasinski et al., 2001). The advancement and employment of planar flow measurement techniques, such as Particle Image Velocimetry (PIV), has been a key development that has provided valuable insight into the instantaneous turbulent flow structure (Willert et al., 1991). Warholic et al. (2001) used the PIV technique to identify turbulent structures close to the wall that the authors designated as being typical of flows involving Newtonian solvents. These structures were characterized by the ejection of low-momentum fluid to the outer velocity region, or defect region, and by quasi-streamwise vortices. Such structures were recognized as locations of large Reynolds stresses. For high measured drag reduction the authors observed reduction or elimination of the ejections from the wall (Warholic et al., 2001). Liberatore et al. (2004) observed that the presence of polymers lead to a decrease in the frequency and the intensity of large-scale ejections when compared to a Newtonian solvent. The polymer induced drag reduction effect was also found to reduce the small-scale fluctuations, as determined from spectral functions (Warholic et al., 2001), and to reduce the magnitude and frequency of the small-scale eddies (Liberatore et al., 2004). Additionally, large regions of almost unidi-

rectional fluctuating velocity vectors were observed for solutions exhibiting high levels of drag reduction (Liberatore et al., 2004; Warholic et al., 2001).

The aim of this work is to study the effect of drag reducing polymers on the instantaneous structure of turbulent pipe flow and to extend our knowledge to practically relevant conditions with measurements at Reynolds numbers up to $Re = 210\,000$. Three different molecular lengths, and thus three different corresponding weights, of the same linear drag reducing polymer (polyethylene oxide, or PEO) have been studied. The Newtonian character of the polymer solutions was first verified by rheological measurements. A pressure-driven horizontal pipe flow apparatus was then used to generate the turbulent flow, and to measure pressure drops over a range of flow-rates. The turbulent flow was characterized with the use of a PIV system.

In the sections below, firstly, the rheological and drag reduction measurements are reported for the various polymers, at different concentrations, over the investigated range of Reynolds numbers. We then present corresponding profiles of the mean flow velocity and of the root mean square (rms) of its fluctuations and, based on the former, measures of the thickness of the buffer layers. This is followed by a presentation of instantaneous images of the turbulent flow with and without the polymer additives. The main contribution of the current study is the uncovering of the presence of two distinct momentum regions of turbulent pipe flow for solutions containing polymer additives, separated by a thin interface layer that is associated with high strain (and shear). It will be shown that these flow structures (i.e. thin layers) propagate far from the wall towards the center of the pipe flow, within an overall region that is larger than that which is investigated typically in

turbulent drag reduction studies (e.g. by numerical simulations due to the computational cost). Finally, the spanwise extent of the regions within which these layers are found is correlated to the level of independently measured drag reduction, and also compared to the extent of the velocity buffer layer.

2. Experimental methods

2.1. Drag reducing polymers

Three different molecular lengths and thus also weights of polyethylene oxide (PEO) were chosen for this investigation. PEO is a linear non-ionic water soluble polymer. All three PEOs were purchased from Sigma-Aldrich, Inc. (Steinhelm, Germany). The molecular weights as given by the manufacturer are 2×10^6, 4×10^6 and $8 \times 10^6\,\mathrm{kg{\cdot}mol^{-1}}$ and the corresponding abbreviations used in the following text are PEO2, PEO4 and PEO8, respectively. Tap water was used throughout as the solvent.

During the dissolution, the polymer powder was sprinkled over a large solvent area and care was taken so that the polymer powder would not clump together on the solvent surface. Polymer powder was weighed with an accuracy of $\pm\,0.1\,\mathrm{mg}$ using an analytical balance (Sartorius MC1 Analytic AC 120S, Illinois, USA). The studied concentrations of the polymer solutions were $c = 5$, 10, 25, 50, 75, 125 and 250 wppm, which correspond to 1.5, 3.0, 7.5, 15.0, 22.5, 37.5 and 75.0 g for 300 L of water used in the experiments.

The apparent shear viscosities of the resulting solutions were characterized using a Physica MCR301 rheometer (Anton-Paar GmbH, Graz, Austria) equipped with a cone and plate measuring geometry. The cone diameter and angle were 60 mm and $1\,^\circ$, respectively. The plate was thermally controlled by a Peltier system and a constant temperature of $25 \pm 0.05\,^\circ\mathrm{C}$ was maintained during the measurements. The apparent shear viscosity μ was measured over a linearly increasing strain rate $\dot{\gamma}$ from 10 to $2\,000\,\mathrm{s^{-1}}$. The data were recorded and evaluated using the Rheoplus software supplied by the manufacturer (Anton Paar Germany GmbH, Ostfildern, Germany). The viscosity

results are presented in Section 3.1.

2.2. Apparatus and drag reduction measurements

A schematic of the experimental flow facility used for the drag reduction characterization and the turbulent flow measurements is shown in Fig. 1. A detailed description of the facility can be found in Zadrazil (2011). The system comprises a 350 L mixing tank, a 300 L pressure vessel, a stainless steel horizontal pipe test section of length $L = 8\,\mathrm{m}$ and inner diameter $D = 25.3\,\mathrm{mm}$, and a drain tank connected to a re-circulation pump (March May Ltd., Huntingdon, UK). The amount of water used for the preparation of polymer solutions was measured with a turbine flowmeter (EW-05611-22, Cole-Palmer, Illinois, USA). The pressure vessel was used instead of a centrifugal pump to drive the flow in order to minimize the mechanical degradation of the polymer. The outlet pipe from the pressure vessel had an inner diameter of 50.8 mm and contained a flow straightening section incorporating a honeycomb. The transition between the outlet pipe and the test section consisted of a smooth contraction. The flow-rate in the outlet section was set by an air valve and a digital pressure sensor inside the pressure vessel that ensured that a constant pressure was kept in the pressure vessel to within $< 0.01\,\mathrm{bar}$ during a run. The flow-rate was then measured by a magnetic-inductive flow meter (Sitrans FM Magflo MAG 5000, Siemens, Denmark) with an accuracy of 0.5% and a repeatability of $< 0.5\%$, as stated by the manufacturer. The overall experimental repeatability, and hence our ability to set a particular flow-rate, velocity and Reynolds number, was quantified directly in our experiments and found be 1.7% at the 95% confidence level.

The macroscale Reynolds number Re based on the bulk velocity U_{bulk}

and pipe diameter D is given by,

$$Re = \frac{\rho U_{\text{bulk}} D}{\mu}, \tag{1}$$

where ρ is the density of the solution (i.e. of water), U_{bulk} is the bulk velocity in the test section (volumetric flow-rate over the cross-sectional flow area $\pi D^2/4$), D is the pipe inner diameter and μ the dynamic (absolute) viscosity from direct measurements (see Section 3.1). Five flow-rates were investigated in this work, which correspond to bulk velocities $U_{\text{bulk}} = 1.5\,\text{m}\cdot\text{s}^{-1}$, $3.0\,\text{m}\cdot\text{s}^{-1}$, $4.5\,\text{m}\cdot\text{s}^{-1}$, $6.0\,\text{m}\cdot\text{s}^{-1}$ and $9.0\,\text{m}\cdot\text{s}^{-1}$, and Reynolds numbers $Re = 3.5 \times 10^4$, 7.0×10^4, 1.1×10^5, 1.4×10^5 and 2.1×10^5, respectively.

The pressure drop along the test section was monitored continuously with membrane differential-pressure transducers (Deltabar S, Endress+Hauser, Germany). The pressure drop Δp was measured between a reference tap located 1.76 m from the test section inlet, and measuring taps at 1.96, 2.96, 3.96, 4.96 and 5.96 m from the same location. Figure 2 confirms from direct pressure tap measurements that the pressure drop in the flow direction is linear, as expected for fully developed flow. The flow-rate, pressure drop and temperature data were automatically recorded at a sampling rate 10 Hz. The level of drag reduction was calculated as follows,

$$DR = \left(\frac{f_{\text{wat}} - f_{\text{add}}}{f_{\text{wat}}} \right)_{Re=\text{const}}, \tag{2}$$

where f is the Fanning friction factor, subscripts 'wat' and 'add' stand for a pure solvent flow and a flow of solvent containing polymer additives, respectively, and 'Re = const' signifies the fact that the comparison is made between flows with the same Re. The Fanning friction factor was calculated

directly from the differential pressure and flow-rate measurements,

$$f = \frac{\Delta p}{\frac{1}{2}\rho U_{\text{bulk}}^2} \frac{D}{4L}. \tag{3}$$

2.3. Flow visualization and PIV measurements

A visualization cell machined from Perspex to the same inner diameter as the main pipe section was located 6.11 m (or 242 D) from the entrance to the pipe. The refractive indices of the visualized fluid (water) and the cell material were 1.33 and 1.48, respectively. The sides of the visualization cell through which the light passed (from the laser light source and to the imaging camera) were flattened and polished, and the camera was placed at right angles to the flattened viewing surface of the cell. This practice minimized the reflections from the curved surfaces and also alleviated optical distortions caused by the difference in the refractive index of the cell material and air. Any remaining distortions caused by the difference between the refractive index of the cell and the contained water were removed by applying a post-processing correction technique. The technique involved the imaging of a highly resolved square grid with thin 0.1 mm crosses printed at a spacing of 0.5 mm on a target plate. The target plate was positioned inside the pipe, along its centerline and within the measurement (laser) plane to within 0.5 mm with the help of the laser sheet. The pipe was then filled with water. Resulting images of the grid were taken and used to transform and correct (de-warp) later images that were taken during the main measurement runs with the target plate removed. This was done systematically with a dedicated function of the laser/camera control software provided by the manufacturer. After correction the software algorithm returned images with a discrepancy

of 1.3 pixels or 33 μm from the known undistorted target grid.

The turbulent flow measurements were performed using a PIV system manufactured by LaVision GmbH (Göttingen, Germany). The system employs a double-pulsed Nd:YAG laser (Nano-L-50-100PV, Litron Lasers Ltd., Rugby, UK) with an emission wavelength of 532 nm. The laser pulse duration is 4 ns, the maximum energy of the pulse 50 mJ and the maximum frequency 100 Hz. During the PIV measurements inert particles were introduced in the flow and the flow is illuminated by a laser sheet. The elastically scattered light is recorded by a camera positioned at 90 ° to the laser light sheet, as detailed in the previous paragraph. In this study, hollow borosilicate glass spheres were used as seeding particles with a mean diameter of $9-13\,\mu$m and density $1\,100 \pm 50\,\mathrm{kg{\cdot}m^{-3}}$, as supplied by LaVision GmbH (Göttingen, Germany). A monochromatic CMOS camera (VC-Imager Pro HS 500; LaVision GmbH, Göttingen, Germany) with a resolution of $1\,280 \times 1\,024$ pixels was used, equipped with macro lenses (EX Sigma DG Marco 105 mm $f/2.8$; Nikon, Japan). The complete area visualized for the PIV was 16.0×12.8 mm, which corresponds to a spatial pixel resolution of 25 μm (see Fig. 3).

During each measurement a set of $500-600$ image pairs was taken at a frequency of 100 Hz. The data were evaluated using the DaVis software supplied by the laser system manufacturer, LaVision GmbH (Göttingen, Germany). After the optical distortion correction, the raw images were preprocessed using an in-built algorithm that subtracted a sliding minimum over three images, which removed any background reflections and increased the signal-to-noise ratio. The images were then processed using a cross-correlation function utilizing a multi-pass technique. During the first pass

the PIV interrogation window was set to 32×32 pixels with 25% overlap of the adjacent areas. The PIV window during the second and third passes was reduced to 16×16 pixels with 50% overlap, while employing information regarding the PIV window displacement from the first pass that was retained. Hence, the PIV vector-to-vector spatial resolution in the final processed result was 0.2 mm. Finally, a median filter was used to reject spurious vectors, which were either replaced by a secondary or ternary cross-correlation peak or interpolated from the neighbour valid vectors.

The turbulent flow field was investigated in terms of instantaneous velocity, velocity fluctuations, streamwise shear strain and two dimensional (2D) vorticity. The instantaneous 2D local flow speed is defined as,

$$U\left(x,y,t\right) = \sqrt{u^2\left(x,y,t\right) + v^2\left(x,y,t\right)}, \tag{4}$$

where u and v are the instantaneous streamwise and spanwise velocity components, respectively. The instantaneous temporal fluctuations of velocity u' and v' are defined from Reynolds decompositions:

$$u\left(x,y,t\right) = \overline{u}\left(x,y\right) + u'\left(x,y,t\right), \tag{5}$$

$$v\left(x,y,t\right) = \overline{v}\left(x,y\right) + v'\left(x,y,t\right), \tag{6}$$

where $\overline{u}$ and $\overline{v}$ are the time-mean streamwise and spanwise velocities, respectively. Note that the tangential velocity component was not measured here, however, we assume that this is zero in the mean. Finally, the instantaneous streamwise shear strain rate and 2D vorticity are given by:

$$\dot{\gamma}_{xy} = \overline{\dot{\gamma}}_{xy} + \dot{\gamma}'_{xy} = \frac{\mathrm{d}\overline{u}}{\mathrm{d}y} + \frac{\mathrm{d}u'}{\mathrm{d}y}, \tag{7}$$

$$\omega_z = \overline{\omega}_z + \omega'_z = \left(\frac{\mathrm{d}\overline{v}}{\mathrm{d}x} - \frac{\mathrm{d}\overline{u}}{\mathrm{d}y}\right) + \left(\frac{\mathrm{d}v'}{\mathrm{d}x} - \frac{\mathrm{d}u'}{\mathrm{d}y}\right). \tag{8}$$

3. Results and discussion

3.1. Rheology

A rheological characterization was performed in order to assess the Newtonian character of the polymer solutions. All solutions show a linear, flat (zero-gradient) dependency of apparent shear viscosity on strain rate, which is an indicator of Newtonian behaviour. As an indicative result, the apparent shear viscosity μ as a function of strain rate $\dot{\gamma}$ for solutions with different concentrations c of PEO8 from 10 to 250 wppm are shown in Fig. 4(a). Figure 4(b) shows the dependence of the mean apparent shear viscosity of the solution $\langle\mu\rangle$ on polymer concentration c. Each data point here has a viscosity value that is averaged over a range of strain rates up to $\dot{\gamma} = 1\,000\,\mathrm{s}^{-1}$, from data such as that presented in Fig. 4(a). In this paper, where values of dynamic (absolute) viscosity μ are required (e.g. for the evaluation of the Reynolds number Re in Eq. 1, or the normalized distance from the wall y^+ in Eq. 13) we employ this strain-rate averaged value $\langle\mu\rangle$. The addition of polymer results in increased values of the apparent shear viscosity. The increase in the apparent viscosity is greater in the case of the higher polymer molecular weight polymers and at higher polymer concentrations.

3.2. Drag reduction efficiency

The drag reduction efficiency (DR) of each polymer solution was calculated by using Eq. 2 and the results can be seen in Fig. 5. Recall that DR arises by comparing the pressure drop occurring in a pipe containing a polymer solution as a fraction of the pressure drop in the equivalent (i.e. dynamically similar) flow of the pure solvent (water) in the absence of the

polymer, at the same Re. The dependency of DR on polymer concentration follows the classical trend. As expected, DR increases with increasing polymer concentration until a plateau is reached. A further increase of polymer concentration does not lead to a significant increase in DR. Within our range of investigated polymer concentrations the existence of a limiting value was more strongly observed with PEO4 and PEO8 than with PEO2. The level of DR also increases with increasing polymer molecular weight, which is in agreement with previous observations (Bismarck et al., 2005; Virk, 1975). The most significant difference in drag reduction behaviour between the various polymer molecular weights can be seen for relatively low Re. With increasing Re the difference in the ability of the polymer molecules to decrease the frictional drag decreases with respect to their molecular weight.

Experiments to assess polymer degradation have also been carried out in which the polymer solutions with the highest polymer concentrations (i.e. $c = 250\,\mathrm{wppm}$) were recirculated $10\times$ through the test section. The evolution of DR for PEO2, PEO4 and PEO8 at $Re = 210\,000$ as a function of number of runs through the test section is shown in Fig. 5. The level of DR decreases with the number of runs in the test section, which suggests mechanical degradation of the polymer molecules. The lines in Fig. 5 are fits to the data using a mathematical model that describes a relationship between DR and polymer degradation developed by Brostow (1983),

$$\frac{DR\,(t)}{DR_\mathrm{o}} = \frac{1}{1 + W\,(1 - e^{-ht})}, \tag{9}$$

where $DR\,(t)$ is the value of DR at time t, DR_o is the initial $DR\,(t = 0)$, W is related to the number of points in a polymer molecule that are vulnerable

to mechanical degradation and h is the decay constant. The parameter W attains values of 1.07, 1.48 and 1.78 for PEO2, PEO4 and PEO8. In addition, the value of W corresponds to a representative average number of times a polymer molecule is broken up in turbulent flow and it amounts to 1, 1.5 and 1.75, respectively. Therefore, the results generated at $c = 250\,\mathrm{wppm}$ imply that as the length of the studied polymer molecules increases (PEO2 < PEO4 < PEO8) so does its vulnerability to mechanical degradation.

The pressure drop data shown in Fig. 5 in the form DR as a function of polymer concentration c for the various investigated polymers and Re, are also presented in the Prandtl–von Kármán plot (i.e. $f^{-0.5}$ *vs.* $Re \cdot f^{0.5}$) in Fig. 6, where: (i) represents laminar flow, (ii) represents turbulent flow of Newtonian fluid and (iii) the maximum DR asymptote as described by Virk (1975). The area between the curves (ii) and (iii) is the drag reduction region. As expected, the results for the pure solvent (water) closely follow the turbulent flow line. When polymer additives are present in the flow the friction factor decreases, which is reflected by an upward shift to higher $f^{-0.5}$ values. The deviation from a straight line that can be seen, e.g. for high concentrations of PEO8, can be attributed to mechanical degradation of polymer molecules (Elbing et al., 2009; Vanapalli et al., 2005). Nevertheless, it should be noted that the current paper deals with the correlation between the instantaneous velocity fields and the measured drag reduction, irrespective of the observed level of polymer degradation.

3.3. Mean velocity profiles

Figure 7 shows spanwise profiles of normalized mean velocity U^+ for PEO2, PEO4 and PEO8 at varying concentrations c. Results are presented

at the lowest and the highest Re used in this work. The mean velocity profiles are normalized by the frictional velocity u_τ, which is defined as,

$$u_\tau = \sqrt{\frac{\tau_\mathrm{w}}{\rho}}, \tag{10}$$

and where the shear stress at the wall ($y = 0$), τ_w, is calculated directly from the differential pressure drop measurements used for the measurement of DR (and mentioned in Section 2.2). Specifically, it is calculated from,

$$\tau_\mathrm{w} = \Delta p \left(\frac{D}{4L} \right). \tag{11}$$

Thus, the normalized mean velocity U^+ and the normalized distance from the wall y^+ are defined as follows:

$$U^+ = \frac{\overline{u}}{u_\tau}, \tag{12}$$

$$y^+ = \frac{y\,\rho u_\tau}{\mu}, \tag{13}$$

for which mean viscosity values μ are taken directly from the rheological measurements presented in Section 3.1.

In this series of plots the spanwise profiles of normalized mean velocity U^+ for the water flows follow closely the theoretical curves for: (i) the viscous sublayer, $U^+ = y^+$ for $y^+ < 5$; and (ii) the log-law region, $U^+ = 2.5\,\ln y^+ + 5.5$ from $y^+ > 30$ to about $y/D \approx 0.3$. In addition, the corresponding profiles for the polymer solution flows are consistent with previous observations (Warholic et al., 1999; Ptasinski et al., 2001). It can be seen that, in agreement with previous studies, increasing DR levels lead to a thickening of the

buffer layer such that the log-law region is shifted to higher values of U^+ and farther away from the wall at $y^+ = 0$. At the maximum DR the log-law region disappears and the velocity profiles follow the empirical relation: (iii) $U^+ = 11.7 \ln y^+ + 17.0$, as described by Virk (1975).

It is useful at this point to quantify the aforementioned thickening of the buffer layer. For this purpose we define the spanwise extent of the buffer layer as the distance from the wall to the intercept between the measured log-law velocity profile for each flow and Virk's theoretical asymptote. Note that we do not assume that the slope of the log-law profile for the polymer solutions is the same as it is for the Newtonian fluid, but rather, we extrapolate the linear region in each U^+ *vs.* y^+ dependency towards Virk's maximum drag reduction profile. Figure 8 shows the buffer layer spanwise extent as a function of the independently measured level of drag reduction DR. The extent of the buffer layer y_{bfl} is expressed normalized by the frictional velocity u_τ and viscosity μ, in a similar manner to Eq. 13. At zero DR (i.e. for water), y_{bfl} is found to be 11.7, in good agreement with the height at which the theoretical relations of the viscous sublayer and of the log-law velocity meet. It can be seen that the normalized extent of the buffer layer y^+_{bfl} is well correlated to the level of drag reduction DR. Interestingly, data points obtained over the studied range of polymer molecular weights, concentrations c and Reynolds numbers Re collapse onto a single trendline with an increasing gradient.

3.4. Velocity fluctuations

Figure 9 shows an extensive comparison of the magnitude of the streamwise velocity fluctuations u' obtained in this work with previously published results (den Toonder et al., 1997; Durst et al., 1995; Hoyer et al., 1996; Kim

et al., 2004, 2007; Ptasinski et al., 2001; Warholic et al., 1999; White et al., 2004). The streamwise velocity fluctuations u' and the distance from the wall y are shown in frictional velocity normalized coordinates u'^{+} and y^{+}. The normalized velocity fluctuations are defined as,

$$u'^{+} = \frac{u'}{u_\tau}. \tag{14}$$

The results of the present study are in good agreement with the published data down to $y^{+} = 10.8$, which corresponds to a distance from the wall of $y = 0.07\,\mathrm{mm}$. This agreement provides added confidence in the accuracy of our data that will be used in the following sections to further examine the characteristics of the flow. It is pointed out that in our study it was not deemed necessary to extend to near-wall measurements. On the contrary, the requirement was to supply global observations of the instantaneous turbulent flow over the whole range $y/D = 0.0 - 0.6$.

3.5. Phenomenological observations of the appearance of shear layers

Examples of instantaneous turbulent flow field measurements for $Re = 35\,000$ are shown in Figs. 10, 11 and 12. In the velocity fluctuation vector-map images, denoted as subplots (d) in these figures, reference vectors having a magnitude of $0.5\,\mathrm{m{\cdot}s^{-1}}$ are shown in the top left corners of the images. The direction of the flow is from left to right and the pipe wall is located at the top of the images. Figures 10 and 12 were constructed from stitching together three consecutive instantaneous images in order to track the evolution of any flow structures or patterns. This was done on the basis that successive PIV images were generated at 10 ms intervals (a frequency of 100 Hz), which is

shorter than the average longitudinal (streamwise) advection time through each one of these images of 11 ms. The advection time is based on the length of the field of view along the flow direction (the 16 mm image width) and the bulk velocity of $U_{\mathrm{bulk}} = 1.5\,\mathrm{m{\cdot}s^{-1}}$ corresponding to $Re = 35\,000$.

In the case of water (Fig. 10) the instantaneous velocity increases from zero at the wall towards the center of the pipe. The instantaneous streamwise strain rate $\dot{\gamma}_{xy}$ and 2D vorticity ω_z show increased values in the wall region where the boundary between the viscous sublayer and the turbulent flow is located. However, in this work we are concerned primarily with flow away from the near-wall area and into the outer region. Away from the immediate vicinity of the wall, towards the center of the pipe, the instantaneous $\dot{\gamma}_{xy}$ and ω_z maps show only random small scale fluctuations without defining features. The vector field of the velocity fluctuations shows a high degree of complexity ranging from the smallest resolved scales to structures that are larger than the radius of the pipe. The large scale velocity structures were previously identified as large contributors to the Reynolds stress (Nakagawat et al., 2001; Warholic et al., 2001).

Instantaneous images of the flow at $Re = 35\,000$ with added drag reducing polymers are shown in Figs. 11 and 12. Figure 11 depicts a single instantaneous turbulent flow field snapshot of PEO8 solutions with polymer concentrations $c = 25$, 50 and 125 wppm. Figure 12 contains a sequence of three stitched consecutive images of the flow of a PEO8 solution at a concentration of $c = 250$ wppm. The measured levels of DR were 51, 56, 69 and 68% for $c = 25$, 50, 125 and 250 wppm, respectively.

The introduction of drag reducing additives results in an abrupt change in

the instantaneous velocities over a short distance and the appearance of: (1) thin filament-like regions associated with high values of instantaneous streamwise shear strain rate $\dot{\gamma}_{xy}$; (2) thin filament-like regions associated with low (large negative) values of instantaneous 2D vorticity ω_z; and (3) extended (with respect to the equivalent pure water flows) regions having unidirectional velocity fluctuations, implying a level of flow correlation or coherence. The described features were not present in all instantaneous images, but their frequency of occurrence increased and their intensity intensified with increasing polymer molecular weight and concentration. In the extreme case of the largest polymer molecular weight PEO8 with the highest concentration of $c = 250\,\mathrm{wppm}$, the above features appeared almost continuously over time.

These features indicate that there is a relatively sudden separation between the high-velocity (high-momentum) flow located around the axis of symmetry of the pipe from the low-velocity (low-momentum) flow in the vicinity of the wall. The observed low- and high-momentum regions are separated by thin filament-like regions that appear as layers with intense shear and vorticity. The thin separation region will be referred to in the following text as a "shear layer", and can be compared to the well known buffer layer that separates the viscous sublayer from the log-law region, which is visible for the Newtonian solvent as well as for the polymer solutions.

To the authors' best knowledge the specific identification of these shear layers has not been reported previously, even though similar (and potentially, linked) phenomena concerning the effects of drag reducers on the velocity fluctuation maps have been reported (Baik et al., 2005; Kim et al., 2004; Liberatore et al., 2004; White et al., 2004). For instance, we may refer

specifically to similar localized "thread-like" features reported in Kim et al. (2004). However, there are noteworthy differences between the two studies and the two observed features. Firstly, our study concerns the flow of a completely pre-diluted (homogeneous) polymer solution with a maximum concentration of 250 wppm, whereas that of Kim et al. (2004) involved the localized injection, at an angle to main flow, of highly concentrated polymer solutions ($1\,000 - 10\,000$ wppm) into a turbulent channel flow of pure solvent. Unlike in Kim et al. (2004) there is no mixing in the present study between the polymer solution and the main flow, since the polymer is already premixed in the supply tank down to molecular level. Secondly, the structures reported in Kim et al. (2004) concerned the direct observation with optical visualisation and birefringence techniques of physical "lumps" of polymer. On the other hand our shear layers appear in the flow maps (streamwise strain rate $\dot{\gamma}_{xy}$ and 2D vorticity ω_z) and were not observed directly as regions of accumulated polymer. Hence, our layers are an instantaneous spatial feature of the turbulent flow field. The present study moves beyond the previous literature by showing that *flow* structures occur in flows of *homogeneous* PEO solutions, as well as in providing detailed information concerning the characteristics (e.g. spatial thickness) and dynamics (e.g. propagation velocity) of these structures and the regions within which they are observed.

In the case of the velocity fluctuation vector maps, such as those in Figs. 11(d) and 12(d), the magnitude of the spanwise velocity fluctuations v' was observed to decrease with increasing polymer concentration c. Visual inspection of videos of the instantaneous velocity fluctuations maps revealed the existence of velocity ejections, i.e. intermittent outward (away from the

wall) vortices of low-velocity fluid, as previously reported in the literature (Warholic et al., 2001). At the highest polymer concentrations the ejections were almost completely suppressed. In addition, it was observed that the small scale vortices were less common in the flows containing drag reduction additives. On the other hand, an increase in the frequency of occurrence and in the size of the unidirectional u'-fluctuation structures can be observed in the vicinity of the wall for solutions containing polymer additives.

The difference between the instantaneous velocity in the low-momentum region and that in the high-momentum region can be seen more clearly in Fig. 13 where profiles of instantaneous velocity are shown for: (a) water, (b) PEO8 at $c = 50\,\mathrm{wppm}$ and (c) PEO8 at $c = 125\,\mathrm{wppm}$; all for $Re = 35\,000$. In the case of water the instantaneous velocity increases gradually from the wall towards the outer velocity-defect region. The addition of polymers causes a separation into low- and high-momentum regions, which is demonstrated by a sudden change of velocity at an interface – the shear layer.

3.6. Shear layer position

The observed shear layers do not appear at a specific location. They are continuously formed in the near-wall region and propagate with time away from the wall with a characteristic velocity such that their position relative to the wall is a random variable. Typical instantaneous images, such as that of vorticity ω_z in Fig. 12 on the bottom left, reveal one or more thin regions (the shear layers) at an angle to the horizontal (flow symmetry axis). Careful observation of the temporal evolution of these layers, that is by slow playback of continuous image sequences for all runs, reveals that they evolve through a competition between the propagation of thin high-strain and high-vorticity

regions outwards and away from the wall towards the pipe centerline, and their simultaneous advection by the mean flow (from left to right in the images shown herein). The end result is a thin filament-like shear layer at an angle α to the flow axis, that propagates outwards from the wall towards the pipe centerline with time and also streamwise position.

Each shear layer will propagate a certain distance from the wall before the levels of strain rate $\dot{\gamma}_{xy}$ and vorticity ω_z decay and it is no longer possible to detect a difference from the rest of the surrounding flow. This maximum distance of the shear layers from the wall that defines the farthest extent of the shear layers from the wall was used to quantify the "shear layer region" thickness. Note that we use the term "shear layer" to refer to the thin region of *instantaneous and localized* intense shear and vorticity (as in Fig. 12(c), bottom left) and the term "shear layer region" to refer to the overall region next to the wall inside which the shear layers exist and propagate.

A Matlab algorithm that was developed in-house was used to filter the salt and pepper noise, and then to detect the shear layer position (and hence the shear layer region thickness) in the maps of instantaneous streamwise shear strain rate $\dot{\gamma}_{xy}$. The procedure is illustrated in Fig. 14. The shear layer thickness $\lambda(x,t)$ was defined as the *most distant* location of the shear layer from the wall at some time t and at some streamwise position x. It should be noted that the regions of high strain immediately next to the wall (i.e. the viscous sublayer) were also included in the calculation. In order to generate independent measurements it must be ensured that the time between successive data points is greater than twice the integral time scale, and the length between adjacent data points is greater than twice the

integral length scale. The integral longitudinal (streamwise) length scale L_x in these turbulent pipe flows, from direct two-point spatial correlations or estimated from temporal correlations using Taylor's hypothesis and the local mean velocity, increases monotonically from zero at the wall to a maximum value at the centreline of about 0.5 to 1 pipe radius $R = D/2$ depending on the Reynolds number (Hassan, 1980; Kim and Adrian, 1999; Sabot and Comte-Bello, 1976). A spatially averaged value relevant to our study would be $0.25 - 0.5\,R$, or $L_x = 3 - 6\,\mathrm{mm}$. Employing an intermediate value for L_x of 4.5 mm and using Taylor's hypothesis gives a corresponding longitudinal integral time scale of $\tau_x = 0.3 - 3\,\mathrm{ms}$ over the range of employed U_{bulk} used in the experiments (i.e. from 1.5 to $9.0\,\mathrm{m{\cdot}s^{-1}}$). These values for L_x and τ_x allow $4 - 5$ measurements per image and the use of consecutive images. The mean shear layer region thickness $\overline{\lambda}$ corresponding to each run (i.e. set of Re, as well as choice and concentration c of polymer) was obtained by averaging over $500 - 600$ images (instantaneous realizations) and $4 - 5$ streamwise positions per image. Hence, each value of $\overline{\lambda}$ reported is an average over at least 2 000 statistically independent shear layer position points λ.

In absolute terms, the resulting mean thickness of the shear layer region $\overline{\lambda}$ is between a factor of 2 and an order of magnitude larger than the mean spanwise extent of the buffer layer y_{bfl} reported previously in Section 3.3. At low levels of DR the ratio $\overline{\lambda}/y_{\mathrm{bfl}}$ is of the order 10 ($\pm\,50\,\%$). Increasing levels of DR lead to increases in both $\overline{\lambda}$ and y_{bfl}, such that at the highest measured DR the two measures approach a ratio $\overline{\lambda}/y_{\mathrm{bfl}}$ of about 2. The largest value of $\overline{\lambda}$ was found to be $0.17\,D$, for PEO8 at $c = 250\,\mathrm{wppm}$ at $Re = 70\,000$.

Figure 15 shows the average thickness of the shear layer region normal-

ized by the pipe diameter ($\overline{\lambda}/D$) as a function of polymer concentration c at different Re for PEO2, PEO4 and PEO8, respectively. Also shown are the normalized average thicknesses of the shear layers regions for the experiments where $c = 250$ wppm polymer solutions were allowed to pass (i.e. re-circulated) $10\times$ through the test section. Zero polymer concentration refers to the pure solvent (water). For each of these polymers the shear layer region thickness $\overline{\lambda}$ increases with increasing polymer concentration c and decreases with increasing Re. Additionally, $\overline{\lambda}$ increases with increasing polymer molecular weight for a given polymer concentration c and Re. During the multi-pass experiments the thickness of the shear layer region decreased gradually with the number of runs through the test section. This decrease can also be seen in Fig. 16 where Probability Density Functions (PDFs) of the thickness of the shear layer region during the multi-pass experiments are shown. The PDFs show that as the number of passes of the polymer solutions through the test section increases (and the independently measured level of DR decreases, see also Fig. 5) the shear layer region is confined increasingly closer to the wall. Recall that the shear layer region is thinnest for flows of the pure solvent when $DR = 0$.

We note, importantly, that the qualitative effects of polymer choice (molecule length, weight), polymer concentration c, Reynolds number Re and the number of runs through the test section on the DR (see Figs. 5 and 15) are very similar to the dependence of the average shear layer region thickness $\overline{\lambda}$ on the same parameters. The similarity suggests that the shear layers are perhaps linked to the underlying mechanism of drag reduction. The relationship between the average shear layer region thickness $\overline{\lambda}$ and the level of DR is

shown more clearly in Fig. 17. In order to account for any Re effects and to remove any related dependence from the presented results, each shear layer thickness is normalized by the corresponding shear layer thickness in a flow of pure solvent (water) at the same Re,

$$\overline{\lambda}_{\mathrm{N}} = \frac{\overline{\lambda}/D}{\left(\overline{\lambda}/D\right)_{\mathrm{wat},Re=\mathrm{const}}}. \tag{15}$$

Shear layers were also identified in the Newtonian flow (water only, without polymer) for which $DR = 0$. The data point on the y-axis (blue filled square) represents a result generated in these flows. The values of $\overline{\lambda}/D$ associated with this data point are 0.0425, 0.0241, 0.0136, 0.0282 and 0.0172 for Re of 35 000, 70 000, 110 000, 140 000 and 210 000, respectively. This is the value used in the denominator of Eq. 15 in order to normalize all other results for the shear layer region thickness in this figure.

On the evidence of Fig. 17, this choice of normalization performs well in collapsing the available data. The thickness of the normalized shear layer region $\overline{\lambda}_{\mathrm{N}}$ increases with increasing level of DR. At low levels of DR this effect is not strong. In the limit of $DR = 0$, when the measurement concerns the value of the shear layer region in the Newtonian flow, the result collapses the value of $\overline{\lambda}_{\mathrm{N}}$ to unity. The shear layer region at $DR = 50\%$ is thickened by about 50% relative to its zero DR value. However, for flows with greater DR, the thickening is much more severe. For the highest measured DR in this work (highest Re with maximum concentration of PEO8) the average thickness of the shear layer region $\overline{\lambda}_{\mathrm{N}}$ increases substantially by up to an order of magnitude when compared to its value at $DR = 0$.

The observation concerning the existence of a possible relationship be-

tween the average thickness of the shear layer region λ and the level of drag reduction DR agrees well with the classical model of DR proposed by Virk (1975), where an increasing level of DR leads to a thickening of the buffer layer. According to this, at the maximum DR the buffer layer reaches the centerline and the classical log-law region disappears entirely.

We emphasise that, although the overall near-wall region within which the shear layers are found (as characterized by $\overline{\lambda}$) extends further away from the wall than the buffer layer, this is in fact the *maximum* extent of the shear layer position relative to the wall. We expect the shear layers to be at some point in their history much closer to the wall than indicated by $\overline{\lambda}$, and also, closer to the buffer region thickness y_{bfl}. Observation of all instantaneous shear layer realisations (i.e. 2D strain rate and vorticity images such as those in Figs. 11 and 12) confirms that the appearance of the *earliest* (closest to the wall) shear layers occurs close to the wall, so that their *minimum* distance from the wall is of the order of y_{bfl}. On the basis that the first appearance of the shear layers occurs at a distance from the wall similar to the buffer layer thickness, it is possible to hypothesise that there is a connection between the thickening of the shear layer regions and the underlying processes of drag reduction and the resulting thickening of the buffer region.

3.7. Shear layer velocity

Finally, we turn our attention to the average angle α between the shear layers and the flow direction. As described previously in Section 3.6, this angle emerges as a region of high strain propagates outwards from the wall towards the pipe centerline while being advected downstream by the flow. Using Taylor's hypothesis of frozen turbulence, the angle α can be converted

to a characteristic velocity of propagation of the shear layers in the spanwise direction away from the wall. Allowing this interpretation, the gradient (i.e. $\tan\,\alpha$) can be thought of as the ratio of this characteristic velocity to the bulk velocity of the flow U_{bulk}.

Figure 18 shows $\tan\,\alpha$ as a function of drag reduction DR. We observe that all data collapse within a constant band of values 0.15 ± 0.02 for DR up to approximately 60%. This suggests that the characteristic velocity of propagation of the shear layers scales well with U_{bulk}, and hence also Re. For higher values of DR there is an indication that the shear layer propagation velocity accelerates, with $\tan\,\alpha$ increasing to a value of 0.2.

This feature of the shear layers, specifically their appearance at an angle to the main flow direction, is similar to the observation made by Christensen and Adrian (2001) in a channel flow who identified a series of "vortex packets" at angle of $12 - 13\,^{\circ}$ (or $\tan\,\alpha = 0.2$) to the main flow direction. Here, the shear layers appear at $\tan\,\alpha = 0.15$, or an angle of $9\,^{\circ}$. However, the present study concerns a liquid flow exhibiting drag reduction in the presence of polymers, whereas Christensen and Adrian (2001) focused exclusively on a gaseous flow of air. We can confirm that, indeed, "vortex packets" have been observed in our flows, but only in our Newtonian water-only flows and were almost entirely absent in our polymer solution flows. Furthermore, the swirling strength at the same spatial locations as those occupied by shear layers does not show a clear, circular vortex core which is the distinctive characteristic associated with vortex packets.

4. Conclusions

The drag reduction efficiency of polyethylene oxide was measured in a turbulent pipe flow over 122 conditions with varying polymer molecular weight, concentration and Reynolds numbers up to 210 000. Different levels of drag reduction were observed with a maximum of 72%. Particle Image Velocimetry was used to assess the effect of the polymer additives on the instantaneous turbulent pipe flow. The presence of the drag reducing polymers was associated with a thickening of the buffer layer and a displacement of the log-law away from the wall, as expected.

An inspection of the instantaneous fields of velocity, velocity fluctuations, 2D vorticity and streamwise shear strain rate revealed that the turbulent pipe flows of polymer solutions undergo what appeared to be a form of separation, whereby low-momentum regions were located in the vicinity of the wall and high-momentum regions were found around the centerline axis. At the interface between the two regions a thin layer of intense vorticity and streamwise shear strain rate was observed that we refer to as a shear layer.

The observed shear layers were not stationary. They were continuously formed close to the wall at a random frequency that increased with increasing polymer concentration and molecular weight. After appearing the layers moved towards the pipe centerline at an angle to the flow direction until they eventually disappeared at some distance. Their characteristic velocity of propagation away from the wall was found to scale well with the bulk flow velocity. Furthermore, a connection was found between the thickness (relative to the wall) of the region within which the shear layers appeared and the measured level of drag reduction. The thickness of the shear layer region

was increased by the presence of polymer additives when compared to the pure solvent. This was similar to the observations relating to the thickening of the buffer layer, however, the shear layer region was considerably thicker (by up to an order of magnitude) than the extent of the buffer layer.

Acknowledgement

The authors gratefully acknowledge the financial support of Halliburton Energy Services.

Figures

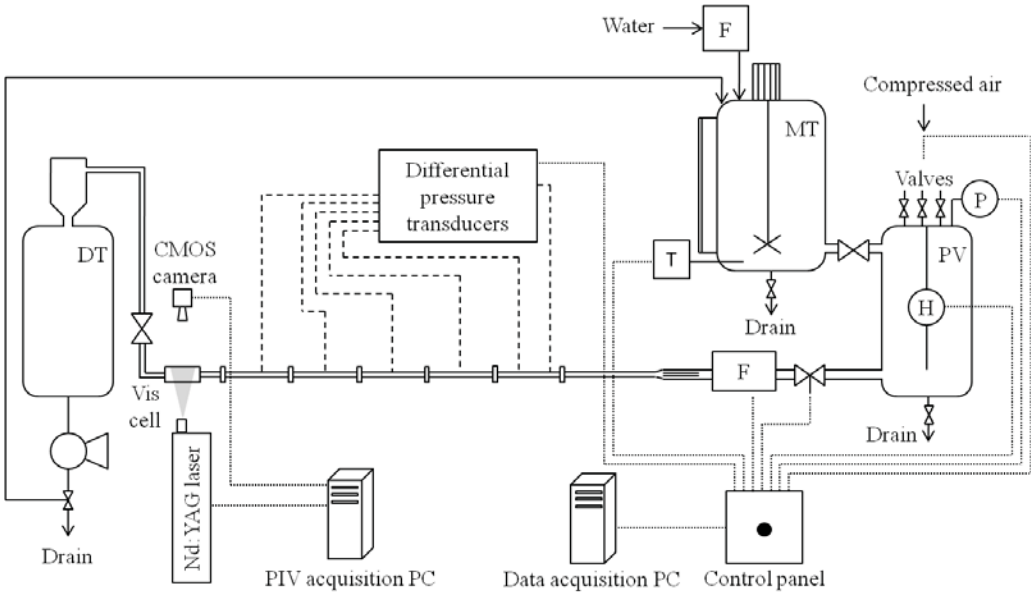


Figure 1: Schematic illustration of the flow facility. The polymer solution is prepared in a mixing tank (MT) and then driven pneumatically through the test section using a pressure vessel (PV). A cyclone is installed on the top of the drain tank (DT) in order to decelerate the flow while minimizing the degradation of the polymers. The instrumentation consists of digital flowmeters (F), pressure transducers (P), temperature sensors (T) and a liquid level meter (H).

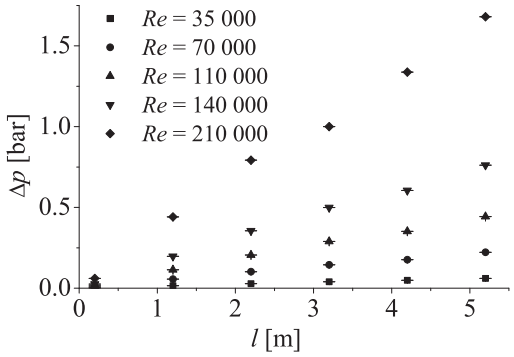
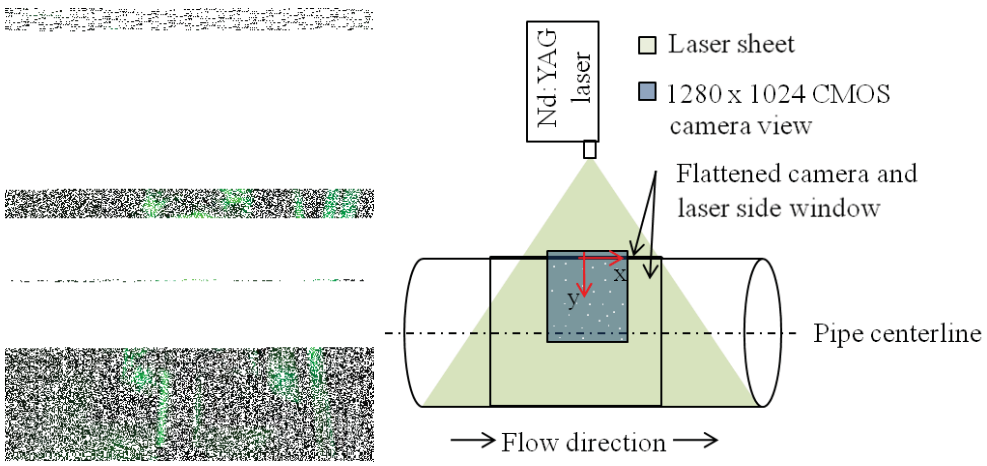
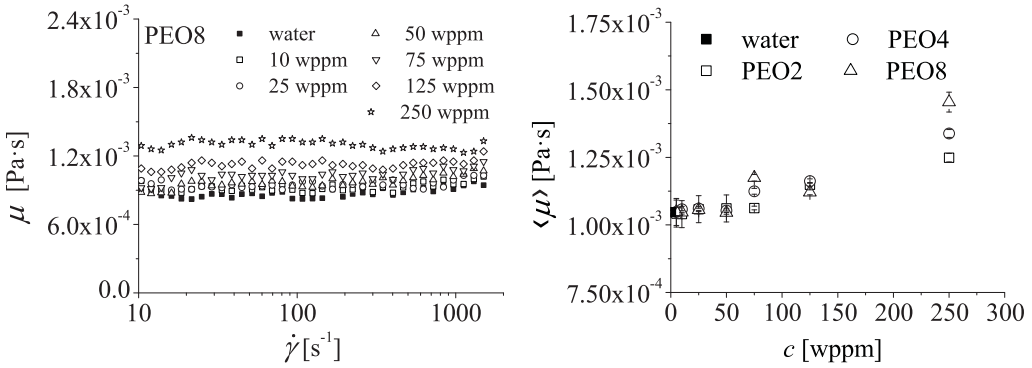


Figure 2: Pressure drop along the length of the test section for water. Also showing the standard error of the differential pressure measurements, which was $< 2\%$ in all cases.



(a) (b)

Figure 3: (a) Photograph and (b) schematic illustration of the visualization cell and the PIV arrangement.



(a) (b)

Figure 4: (a) Dependence of the apparent shear viscosity μ of PEO8 solutions on strain rate $\dot{\gamma}$. (b) Dependence of the mean apparent shear viscosity $\langle\mu\rangle$ (averaged over the range $\dot{\gamma} = 10 - 1\,000\,\mathrm{s}^{-1}$) of PEO2, PEO4 and PEO8 solutions on polymer concentration c, and comparison with pure solvent (water).

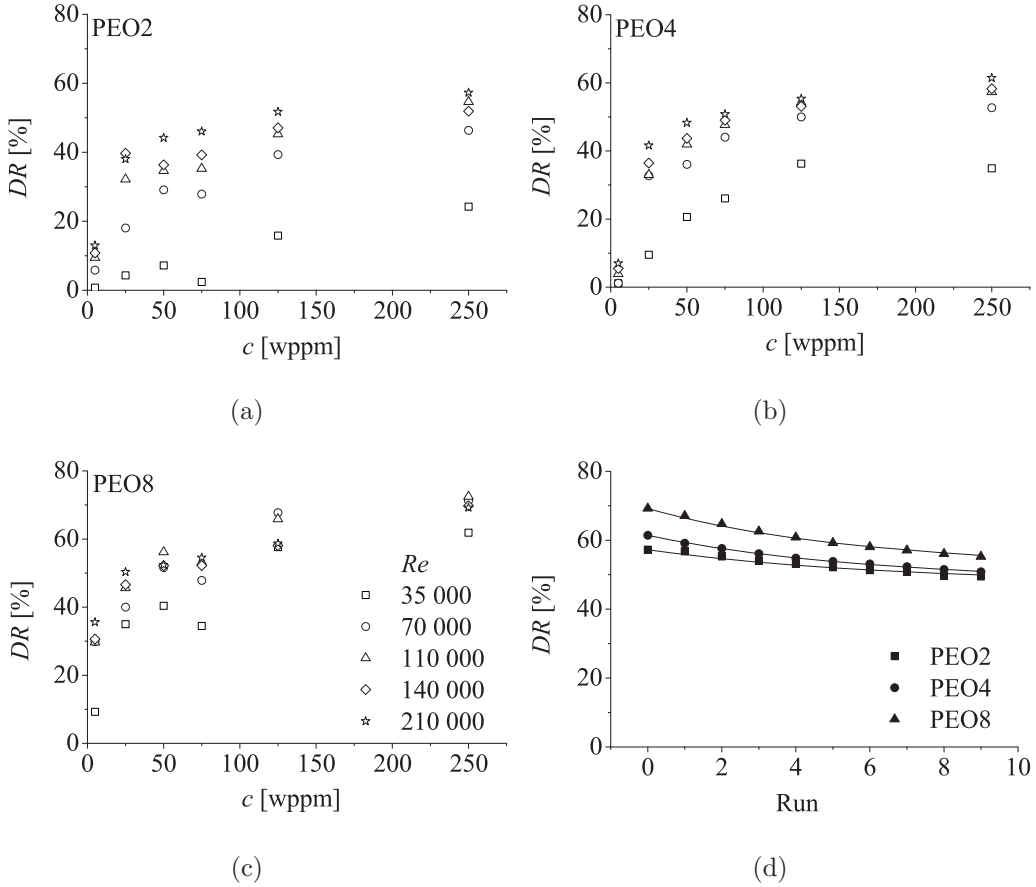


Figure 5: Drag reduction DR (%) as a function of polymer concentration for: (a) PEO2, (b) PEO4 and (c) PEO8, at various Reynolds numbers Re. (d) Dependence of drag reduction DR on the number of runs through the test section for $c = 250$ wppm at $Re = 210\,000$.

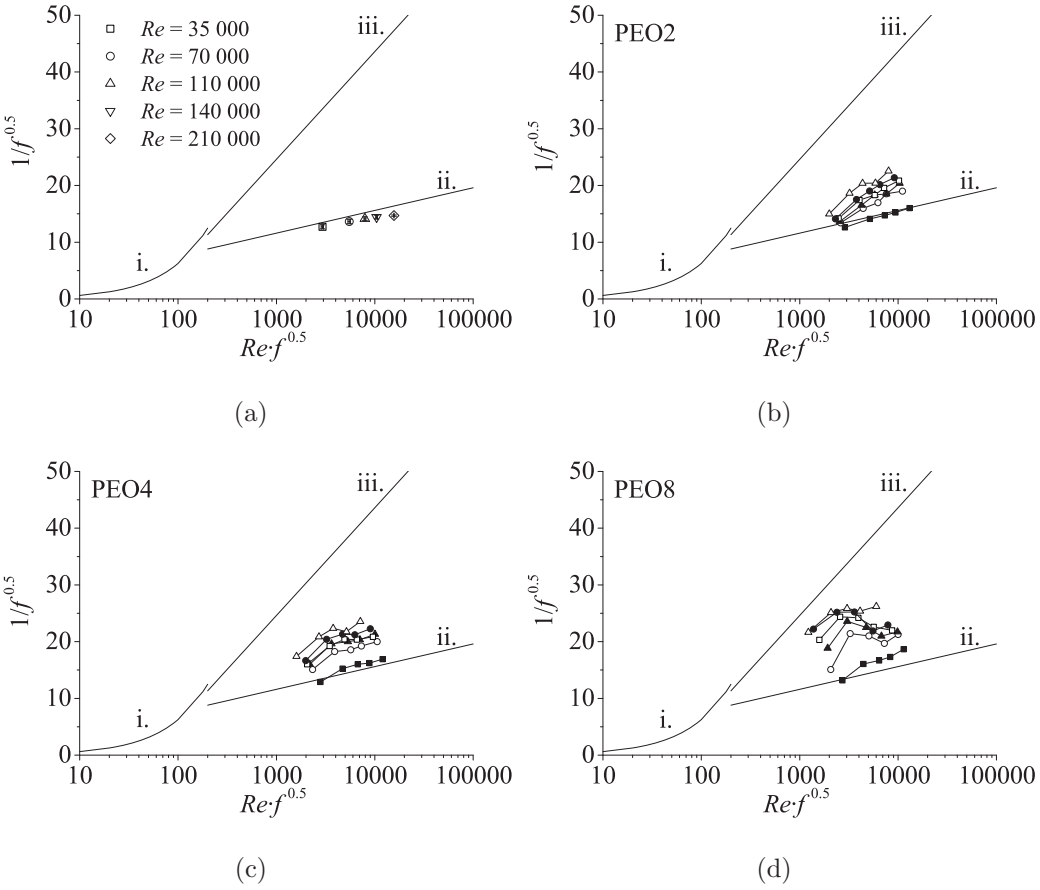


Figure 6: Prandtl–von Kármán plot for: (a) water, (b) PEO2, (c) PEO4 and (d) PEO8.

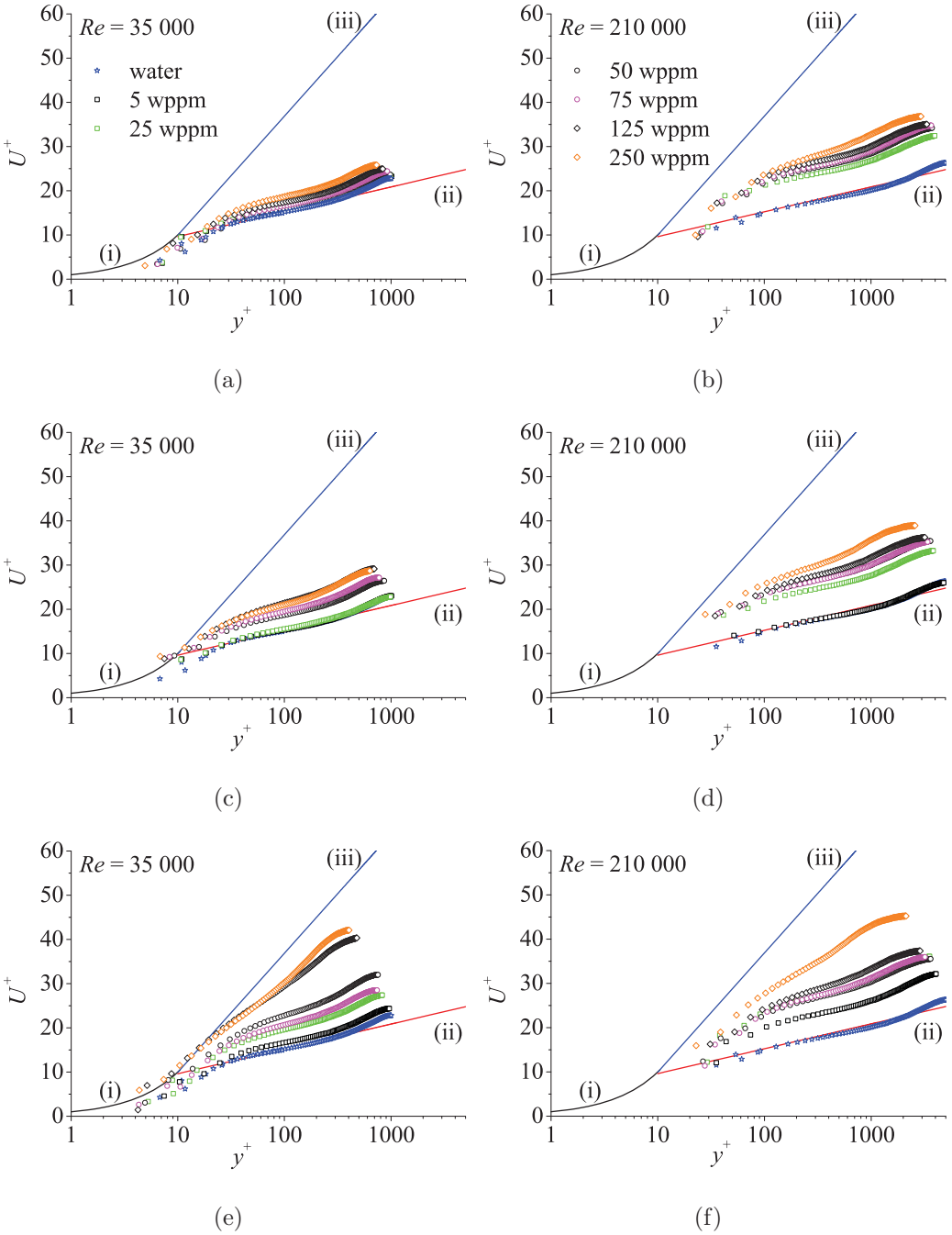


Figure 7: Dependency of the mean velocity normalized by the frictional velocity u'^{+} on the distance from the wall normalized by the frictional velocity y'^{+} for PEO2 (a) and (b), PEO4 (c) and (d) and PEO8 (e) and (f).

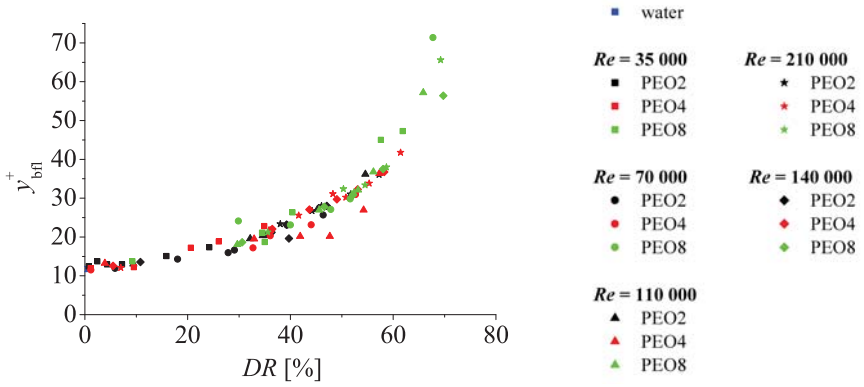


Figure 8: Relation between the thickness of the buffer layer expressed in frictional velocity normalized distance from the wall y^+ and the corresponding measured level of DR.

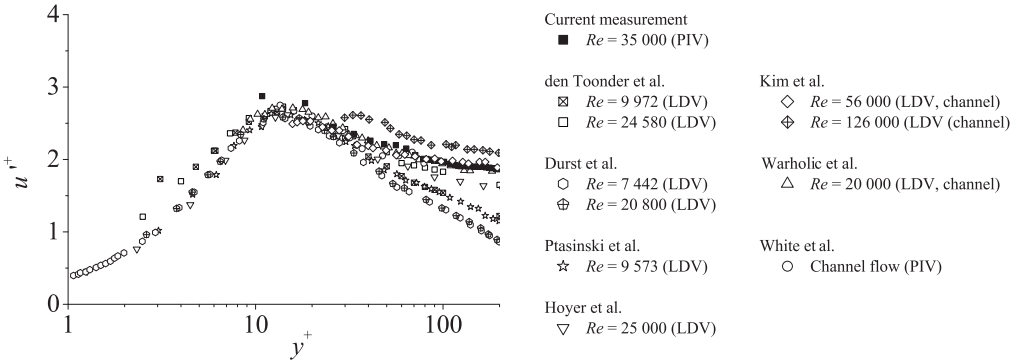


Figure 9: Comparison of the current measurements with published results in terms of the profile of the rms of the streamwise velocity fluctuations normalized by the frictional velocity u'^+ over the distance from the wall normalized by the frictional velocity y'^+ for water.

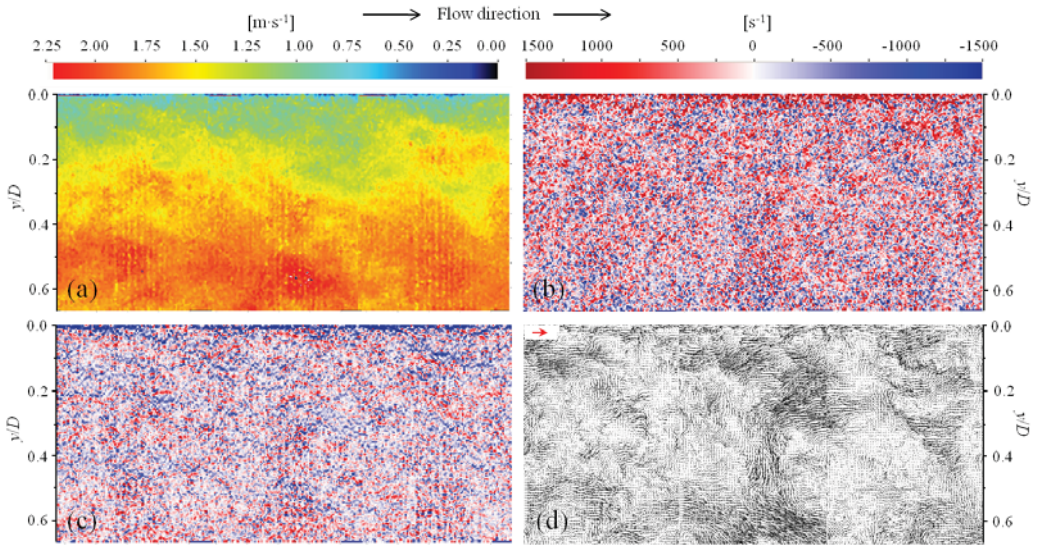


Figure 10: A sequence of instantaneous: (a) local (scalar) speed U, (b) 2D vorticity ω_z, (c) streamwise shear strain rate $\dot{\gamma}_{xy}$ and (d) velocity fluctuation (vector) maps (u' and v'), all for water at $Re = 35\,000$.

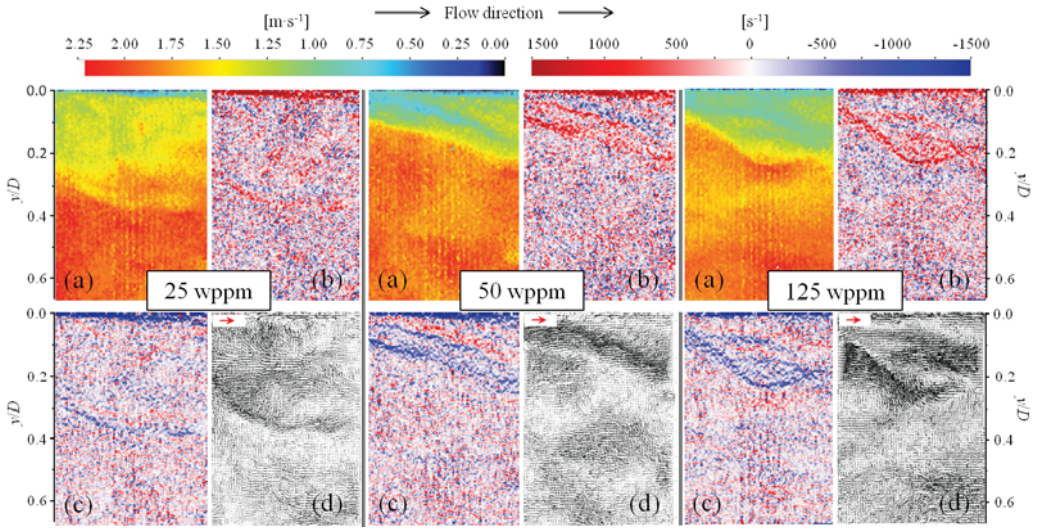


Figure 11: Instantaneous images, similar to Fig. 8, of: (a) local (scalar) speed U, (b) 2D vorticity ω_z, (c) streamwise shear strain rate $\dot{\gamma}_{xy}$ and (d) velocity fluctuation (vector) maps (u' and v'), all for PEO8 at $Re = 35\,000$, with $c = 25$ (left), 50 (center) and 125 wppm (right).

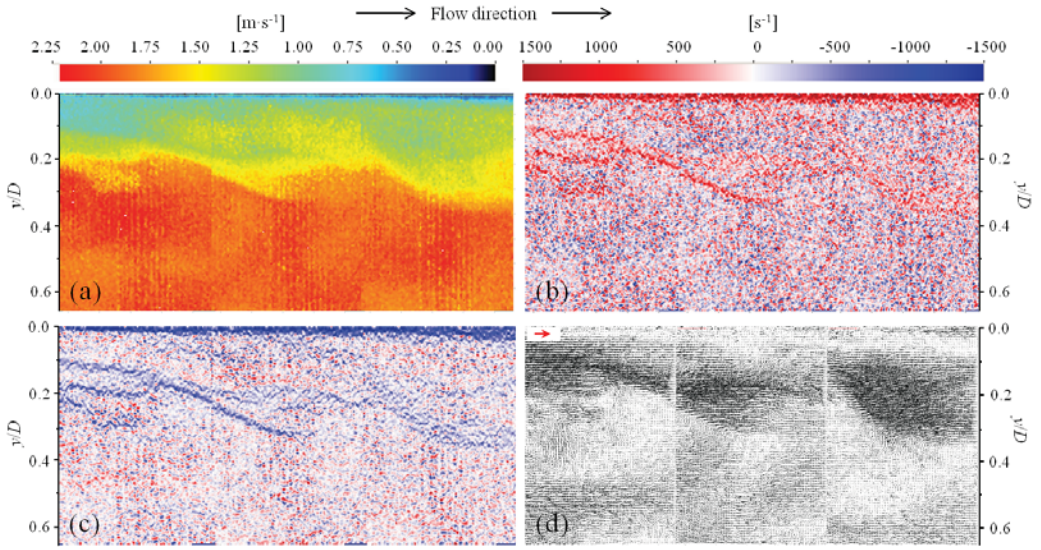


Figure 12: A stitched-together sequence of the instantaneous: (a) local (scalar) speed U, (b) 2D vorticity ω_z, (c) streamwise shear strain rate $\dot{\gamma}_{xy}$ and (d) velocity fluctuation (vector) maps (u' and v'), all for PEO8 at $c = 250$ wppm and $Re = 35\,000$.

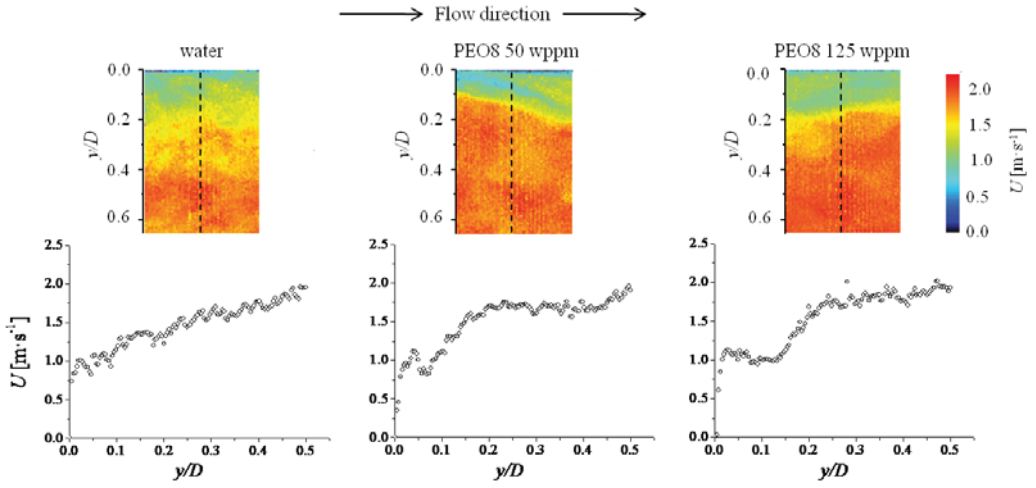


Figure 13: Spanwise profiles of instantaneous speed U for: water (left), PEO8 $c = 50$ wppm (center) and (c) PEO8 $c = 125$ wppm (right), all at $Re = 35\,000$.

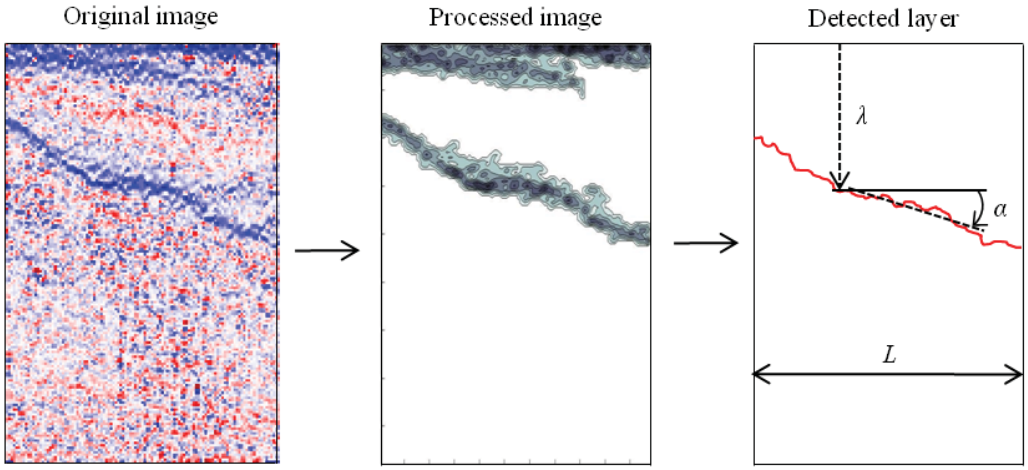


Figure 14: Shear layer detection method with a typical result. Also showing the definitions of relevant quantities as used in Sections 3.6 and 3.7.

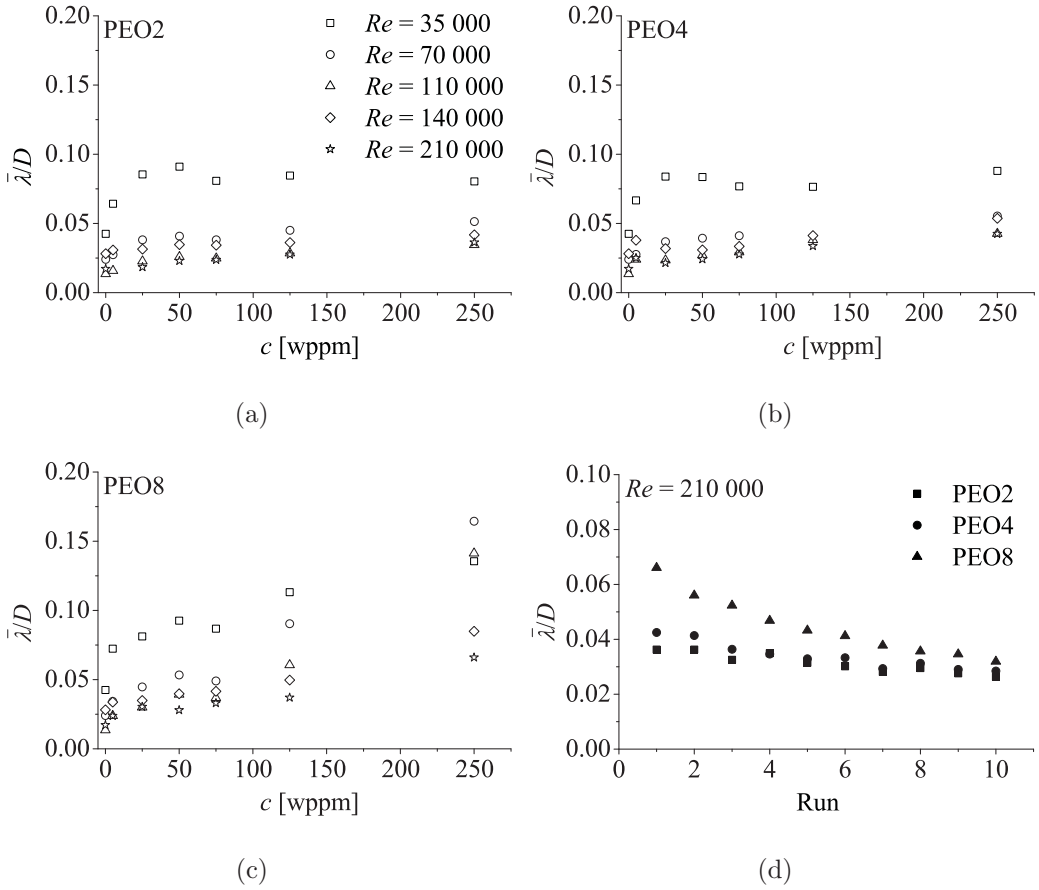


Figure 15: Normalized shear layer region thickness from the wall $\overline{\lambda}/D$ as a function of polymer concentration c for: (a) PEO2, (b) PEO4 and (c) PEO8 at various Reynolds numbers Re. (d) Dependence of the normalized shear layer region thickness $\overline{\lambda}/D$ on the number of runs through the test section for $c = 250\,\text{wppm}$ at $Re = 210\,000$.

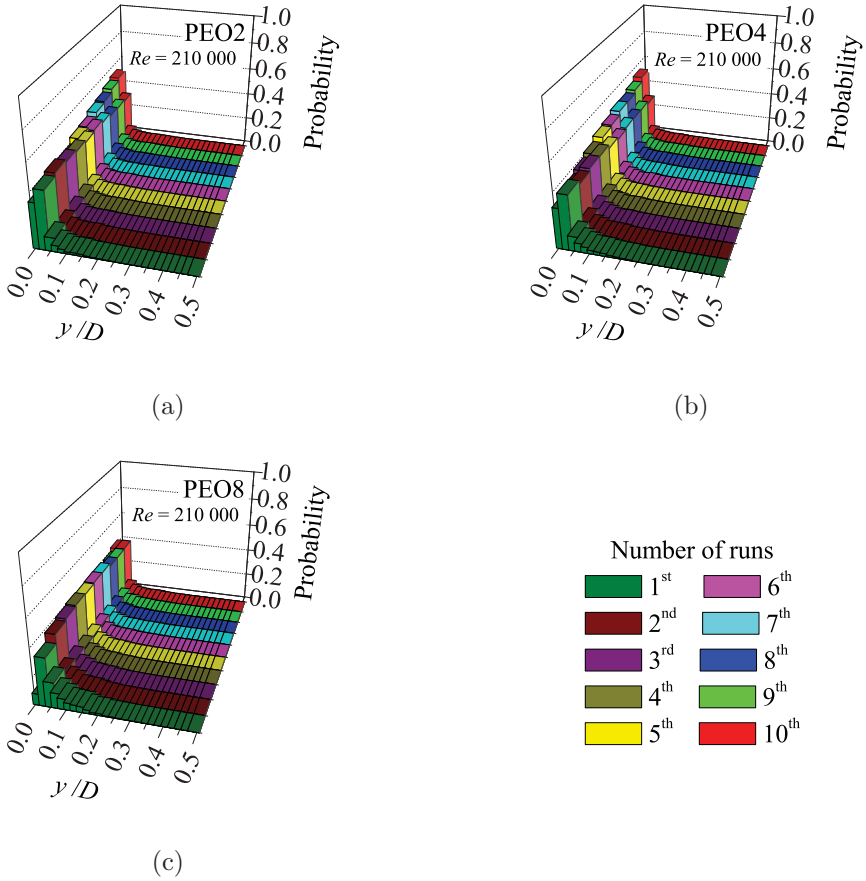


Figure 16: Probability Density Functions of the shear layer region thickness for: (a) PEO2, (b) PEO4 and (c) PEO8. All solutions have the same (maximum) concentration $c = 250$ wppm and were allowed to pass $10\times$ through the test section at $Re = 210\,000$.

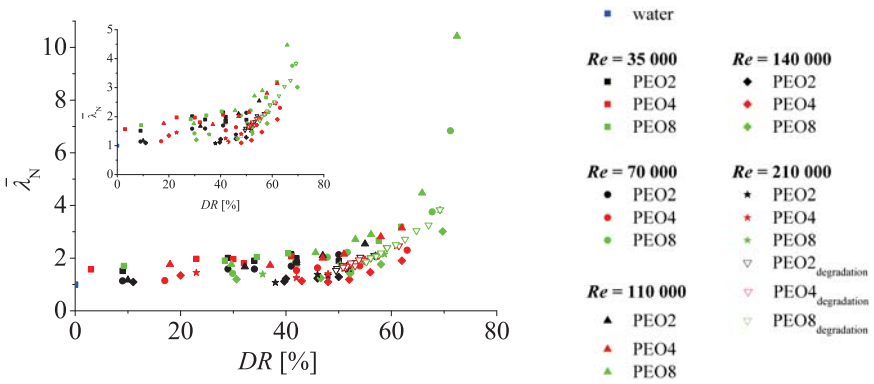


Figure 17: Relation between the normalized shear layer region thickness $\overline{\lambda}_N$ and the corresponding measured level of drag reduction DR. The insert repeats the plot with the vertical axis only up to $\overline{\lambda}_N = 5$. Data points with very high values of $\overline{\lambda}_N$ and DR are not shown here, in order to indicate the trend at lower levels of DR.

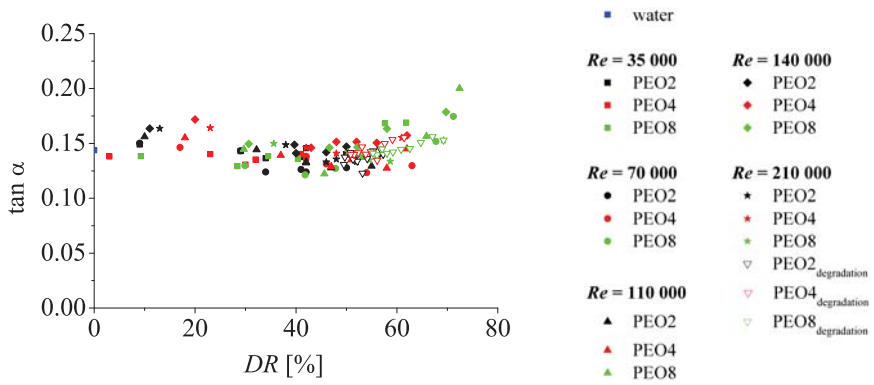


Figure 18: Relation between the mean shear layer gradient and the corresponding measured level of drag reduction DR.

631 Toms, B., 1948. Some observations on the flow of linear polymer solutions
632 through straight tubes at large Reynolds numbers, in: Proceedings of the
633 First International Congress on Rheology. North Holland Publishing Co.,
634 Amsterdam, vol. II, pp. 135-141.

635 Morgan, S.E., McCormick, C.L., 1990. Water-soluble polymers in enhanced
636 oil recovery. Progress in Polymer Science 15, 103-145.

637 Lucas, E.F., Mansur, C.R.E., Spinelli, L., Queiros, Y.G.C., 2009. Polymer
638 science applied to petroleum production. Pure and Applied Chemistry 81,
639 473-494.

640 Burger, E.D., Chorn, L.G., Perkins, T.K., 1980. Studies of drag reduction
641 conducted over a broad range of pipeline conditions when flowing Prudhoe
642 Bay crude-oil. Journal of Rheology 24, 603-626.

643 Singh, R.P., Singh, J., Deshmukh, S.R., Kumar, D., Kumar, A., 1995. Ap-
644 plication of drag-reducing polymers in agriculture. Current Science 68,
645 631-641.

646 Sellin, R.H.J., Ollis, M., 1980. Polymer drag reduction in large pipes and
647 wewers - results of recent fluid trials. Journal of Rheology 24, 967-967.

648 Oliver, D.R., Bakhtiyarov, S.I., 1983. Drag reduction in exceptionally dilute
649 polymer-solutions. Journal of Non-Newtonian Fluid Mechanics 12, 113-
650 118.

651 Virk, P.S., Merrill, E.W., Mickley, H.S., Smith, K.A., 1967. The Toms phe-
652 nomenon: turbulent pipe flow of dilute polymer solutions. Journal of Fluid
653 Mechanics 30, 305-328.

654 Virk, P.S., 1975. Drag reduction fundamentals. AIChE Journal 21, 625-656.

655 Brostow, W., 2008. Drag reduction in flow: review of applications, mecha-
656 nism and prediction. Journal of Industrial and Engineering Chemistry 14,
657 409-416.

658 Lumley, J., Blossey, P., 1998. Control of turbulence. Annual Review of Fluid
659 Mechanics 30, 311-327.

660 White, C.M., Mungal, M.G., 2008. Mechanics and prediction of turbulent
661 drag reduction with polymer additives. Annual Review of Fluid Mechanics
662 40, 235-256.

663 den Toonder, J.M.J., Hulsen, M.A., Kuiken, G.D.C., Nieuwstadt, F.T.M.,
664 1997. Drag reduction by polymer additives in a turbulent pipe flow: Nu-
665 merical and Laboratory Experiments. Journal of Fluid Mechanics 337, 193-
666 231.

667 P.K. Ptasinski, F.T.M. Nieuwstadt, B.H.A.A. Van den Brule, M.A. Hulsen,
668 2001. Experiments in turbulent pipe flow with polymer additives at max-
669 imum drag reduction. Flow Turbulence and Combustion 66, 159-182.

670 Willert, C.E., Gharib, M., 1991. Digital particle image velocimetry. Experi-
671 ments in Fluids 10, 181-193.

672 Warholic, M.D., Heist, D.K., Katcher, M., Hanratty, T.J., 2001. A study
673 with particle-image velocimetry of the influence of drag-reducing polymers
674 on the structure of turbulence. Experiments in Fluids 31, 474-483.

675 Liberatore, M.W., Baik, S., Mchugh, A.J., Hanratty, T.J., 2004. Turbulent
676 drag reduction of polyacrylamide solutions: effect of degradation on molec-
677 ular weight distribution. Journal of Non-Newtonian Fluid Mechanics 123,
678 175-183.

679 Zadrazil, I., 2011. Various aspects of polymer induced drag reduction in tur-
680 bulent flow. PhD thesis, Imperial College London.

681 Bismarck, A., Chen, L., Griffin, J.M., Hewitt, G.F., Vassilicos, J.C., 2005.
682 Role of polymers and surfactants in drag reduction in oil industry appli-
683 cations. Imperial College Consultants Ltd.

684 Brostow, W., 1983. Drag reduction and mechanical degradation in polymer-
685 solutions in flow. Polymer 24, 631-638.

686 White, C.M., Somandepalli, V.S.R., Mungal, M.G., 2004. The turbulence
687 structure of drag-reduced boundary layer flow. Experiments in Fluids 36,
688 62-69.

689 Kim, K., Sirviente, A.I., 2007. Wall versus centerline polymer injection in
690 turbulent channel flows. Flow, turbulence and combustion 78, 69-89.

691 Kim, K., Islam, M.T., Shen, X., Sirviente, A.I., Solomon, M.J., 2004. Effect
692 of macromolecular polymer structures on drag reduction in a turbulent
693 channel flow. Physics of Fluids 16, 4150-4162.

694 Warholic, M.D., Massah, H., Hanratty, T.J., 1999. Influence of drag-reducing
695 polymers on turbulence: effects of Reynolds number, concentration and
696 mixing. Experiments in Fluids 27, 461-472.

Hoyer, K., Gyr, A., 1996. Turbulent velocity field in heterogeneously drag reduced pipe flow. Journal of Non-Newtonian Fluid Mechanics 65, 221-240.

Durst, F., Jovanovic, J., Sender, J., 1995. LDA measurements in the near-wall region of a turbulent pipe flow. Journal of Fluid Mechanics 295, 305-335.

Nakagawa, S., Hanratty, T.J., 2001. Particle image velocimetry measurements of flow over a wavy wall. Physics of Fluids 13, 3504-3507.

Baik, S., Vlachogiannis, M., Hanratty, T.J., 2005. Use of particle image velocimetry to study heterogeneous drag reduction. Experiments in Fluids 39, 637-650.

Christensen, K.T., Adrian, R.J., 2001. Intermittency of coherent structures in the core region of fully developed turbulent pipe flow. Journal of Fluid Mechanics 431, 433-443.

Hassan, Y., 1980. Experimental and modeling studies of two-point stochastic structure in turbulent pipe flow. Ph.D. dissertation, University of Illinois, Urbana, Illinois, USA.

Kim, K.C., Adrian, R.J., 1999. Very large-scale motion in the outer layer. Physics of Fluids 11, 417-422.

Sabot, J., Comte-Bellot, G., 1976. Intermittency of coherent structures in the core region of fully developed turbulent pipe flow. Journal of Fluid Mechanics 75, 767-796.

Vanapalli, S.A., Islam, M.T., Solomon, M.J., 2005. Scission-induced bounds

on maximum polymer drag reduction in turbulent flow. Physics of Fluids 17, 095108.

Elbing, B.R., Winkel, E.S., Solomon, M.J., Ceccio, S.L., 2009. Degradation of homogeneous polymer solutions in high shear turbulent pipe flow. Experiments in Fluids 47, 1033-1044.